BIOCHEMISTRY
including biophysical chemistry & molecular biology

Article

pubs.acs.org/biochemistry

Nuclear Magnetic Resonance Structure of the III−IV−V Three-Way Junction from the Varkud Satellite Ribozyme and Identification of Magnesium-Binding Sites Using Paramagnetic Relaxation Enhancement

Eric Bonneau and Pascale Legault*

Département de Biochimie et Médecine Moléculaire, Université de Montréal, C.P. 6128, Succursale Centre-Ville, Montréal, QC, Canada H3C 3J7

Supporting Information

ABSTRACT: The VS ribozyme is a catalytic RNA found within some natural isolates of *Neurospora* that is being used as a model system to improve our understanding of RNA structure, catalysis, and engineering. The catalytic domain contains five helical domains (SLII−SLVI) that are organized by two three-way junctions. The III−IV−V junction is required for high-affinity binding of the substrate domain (SLI) through formation of a kissing loop interaction with SLV. Here, we determine the high-resolution nuclear magnetic resonance (NMR) structure of a 47-nucleotide RNA containing the III−IV−V junction (J345). The J345 RNA adopts a Y-shaped fold typical of the family C three-way junctions, with coaxial stacking between stems III and IV and an acute angle between stems III and V. The NMR structure reveals that the core of the III−IV−V junction contains four stacked base triples, a U-turn motif, a cross-strand stacking interaction, an A-minor interaction, and a ribose zipper. In addition, the NMR structure shows that the cCUUGg tetraloop used to stabilize stem IV adopts a novel RNA tetraloop fold, different from the known gCUUGc tetraloop structure. Using Mn^{2+}-induced paramagnetic relaxation enhancement, we identify six Mg^{2+}-binding sites within J345, including one associated with the cCUUGg tetraloop and two with the junction core. The NMR structure of J345 likely represents the conformation of the III−IV−V junction in the context of the active VS ribozyme and suggests that this junction functions as a dynamic hinge that contributes to substrate recognition and catalysis. Moreover, this study highlights a new role for family C three-way junctions in long-range tertiary interactions.

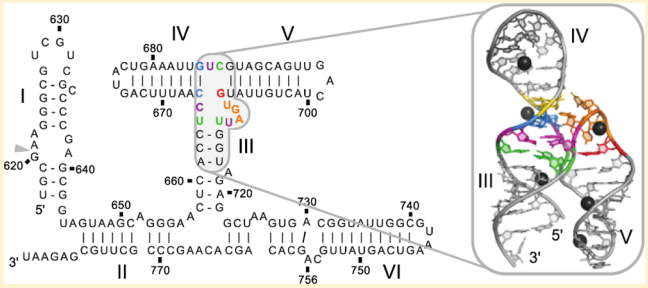

Multiway junctions are ubiquitous structural elements of nucleic acids found in all domains of life that have numerous roles in the dynamic processes of living cells, such as genetic recombination and mRNA splicing. The most abundant forms of RNA junctions are three-way junctions in which three double-stranded helices are connected at the same branch point, and these are found in a plethora of different RNAs.[1−3] Three-way junctions are essential architectural elements that control tertiary structure folding by supporting the packing and positioning of preformed helical domains, and they often promote the formation of remote tertiary interactions. Three-way junctions also play important functional roles because they are key elements for targeting RNA-binding proteins,[4] as well as for forming ligand-binding pockets in riboswitch aptamers[5,6] and for the folding of catalytically active ribozymes.[7,8]

Three-way junctions generally fold in such a way that two of the three helices are coaxially stacked on one another to form a pseudocontinuous helix.[1−3] Topological analyses of known structures of three-way junctions have led to the classification of these junctions into three major families, named A, B, and C.[1] Family C was found to be the most abundant class and the only one containing nonrRNAs. A characteristic feature of family C is that one of the single-stranded regions connecting the three helices is longer than the other two and usually adopts a sharp turn, such as a U-turn or a T-loop. These loop motifs are recurrent in three-way junctions, where they govern the folding of the junction cores and the relative position of the helices.[2] The single-stranded regions connecting the helices may also be involved in base triples and quadruples, as well as A-minor motifs[9] and ribose zippers.[10] Metal cations, typically Mg^{2+} ions, often assist the folding of three-way junctions by stabilizing interactions between distant helices, inducing conformational changes and neutralizing the electrostatic repulsion of negatively charged phosphates that may come into close contact at the junction core.[11−14] Despite this wealth of structural knowledge available on three-way junctions, it is still difficult to predict their structure and metal-binding sites on the basis of sequence alone.

Received: July 4, 2014
Revised: September 4, 2014
Published: September 19, 2014

dx.doi.org/10.1021/bi500826n | *Biochemistry* 2014, 53, 6264−6275

The *Neurospora* Varkud Satellite (VS) RNA is a naturally occurring ribozyme and a member of the family of small nucleolytic ribozymes.[15−20] It catalyzes both cleavage and ligation reactions of a specific phosphodiester bond,[15,21] and metal cations are required for both folding and catalysis.[22−29] The minimal functional VS ribozyme contains six stem−loops (or stems) separated into two functional domains: stem−loop I (SLI) forms the substrate domain, whereas stem−loops II−VI (SLII−SLVI, respectively) define the catalytic domain (Figure 1A).[23] Substrate recognition involves formation of a high-affinity kissing loop interaction between SLI and SLV, and this interaction induces a helix shift in SLI that conformationally activates the substrate for catalysis (Figure 1A).[30−34] Like the hairpin ribozyme, the active site of the VS ribozyme is formed by the interaction of two internal loops, the substrate internal loop of SLI and the A730 internal loop of SLVI.[18,20,35,36] A general acid−base mechanism has been proposed for the VS ribozyme cleavage reaction, with G_{638} of SLI as the general base and A_{756} of the A730 loop of SLVI as the general acid.[35,37−43]

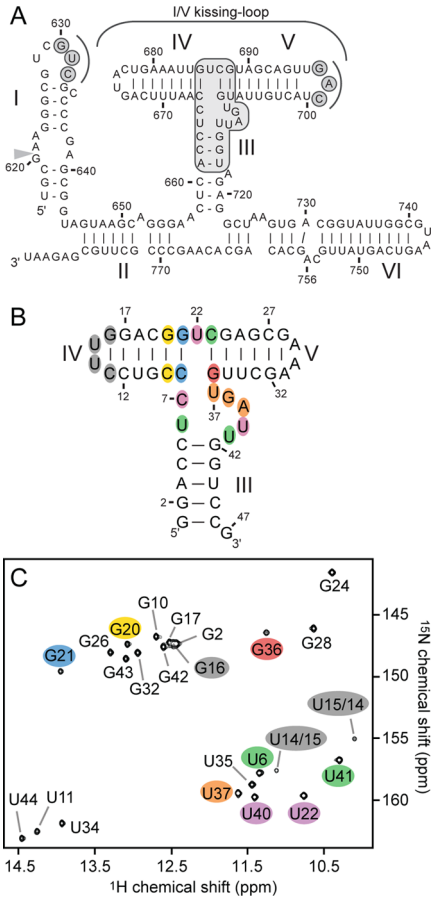

Figure 1. J345 RNA adopts a single stable structure in the presence of Mg^{2+} ions. (A) Sequence and proposed secondary structure of a *cis*-cleaving VS ribozyme (including residues 617−783).[23] The cleavage site is shown with a gray arrowhead. Gray shading is used to highlight the nucleotides involved in WC base pairs at the I−V kissing loop interaction as well as residues from the III−IV−V junction that are present in the J345 RNA. (B) Sequence and proposed secondary structure[23] of the 47-nucleotide J345 RNA used in this study. (C) 2D $^{1}H-^{15}N$ HSQC spectrum of the ^{15}N-labeled J345 RNA in the presence of 5 mM $MgCl_2$. In panels B and C, the shading of residues is color-coded according to structural elements present in the NMR structure (see Figure 3).

In the VS ribozyme, the structure of the catalytic domain is governed by two three-way junctions: the II−III−VI and III−IV−V junctions (Figure 1A).[23] These junctions play a critical role in defining the relative orientation of the connected helices.[44,45] Although the III−IV−V junction is not absolutely required for activity, it is an important architectural domain that mediates recognition of the SLI substrate domain and thereby greatly increases the catalytic activity of the VS ribozyme.[28] Specifically, base substitutions of most of the core residues within the III−IV−V junction interfere with both the cleavage and ligation activities.[38,45,46] Furthermore, three residues in the longest single-stranded region are proposed to form a U-turn motif within the junction core.[46] A family C topology has been predicted for the III−IV−V junction by several laboratories,[1,3] but there is no consensus from these predictions in terms of coaxial stacking, which may involve either stems IV and V[47] or stems III and IV.[1,3] The latter prediction is in agreement with low-resolution models of the VS ribozyme based on fluorescence resonance energy transfer (FRET)[45] and small-angle X-ray scattering (SAXS).[48]

In this study, we determine the nuclear magnetic resonance (NMR) solution structure of the J345 RNA (Figure 1B), a 47-nucleotide RNA that encompasses the VS ribozyme III−IV−V junction. The NMR structure reveals that the J345 RNA adopts a Y-shaped structure that belongs to family C of three-way junctions. The structure of the three-way junction within J345 is stabilized by a complex network of interactions, which includes coaxial stacking of stems III and IV. In addition, we determine that the cCUUGg tetraloop used to stabilize stem IV adopts a structure that is different from the known gCUUGc tetraloop structures. Using Mn^{2+}-induced paramagnetic relaxation enhancement (PRE),[49] we characterize six Mg^{2+}-binding sites within the J345 RNA. Our study provides insights into the global folding of the VS ribozyme, particularly the structural role of the III−IV−V junction in positioning the SLV loop for SLI substrate recognition.

EXPERIMENTAL PROCEDURES

Plasmids and DNA Templates. Double-stranded PCR fragments encoding J345-VS and S3-VS RNAs and flanked by a T7 promoter were inserted into the *Hin*dIII−*Eco*RI sites of the pTZ19R-derived pTR-4 vector[50] to generate the pJ345 and pS3 plasmids, respectively. The J345-VS and S3-VS RNAs correspond to the J345 (Figure 1B) and S3 RNAs (Figure 2), respectively, with a Varkud Satellite (VS) ribozyme substrate at their 3′-ends.[50] Prior to transcription, the plasmids were fully linearized using *Eco*RI (New England Biolabs). For transcription of S12, $S3_{30-38}$, and $S3_{30-40}$ RNAs (Figure 2), partially single-stranded synthetic DNA templates were used (Integrated DNA Technologies).[51]

RNA Synthesis and Purification. Unlabeled, ^{15}N-labeled, and ^{13}C- and ^{15}N-labeled RNAs (J345-VS, S12, S3-VS, $S3_{30-38}$, and $S3_{30-40}$) were synthesized in vitro from their DNA template using a T7 RNA polymerase with an N-terminal His_6 tag prepared in house[52] and the appropriate NTPs, either unlabeled NTPs (Sigma-Aldrich) or isotopically labeled NTPs (^{13}C- and ^{15}N-labeled or ^{15}N-labeled) prepared in house.[53] Following the transcription reactions of J345-VS and S3-VS, 25 mM $MgCl_2$ and purified *trans*-cleaving TR-4 VS ribozyme[50] (1:10 VS ribozyme:full-length transcribed RNA molar ratio) were added to the transcription mixtures and incubated for 8 h at 37 °C to produce the J345 and S3 RNAs with homogeneous 3′-ends. J345, S12, and S3 RNAs were treated with calf

dx.doi.org/10.1021/bi500826n | *Biochemistry* 2014, 53, 6264−6275

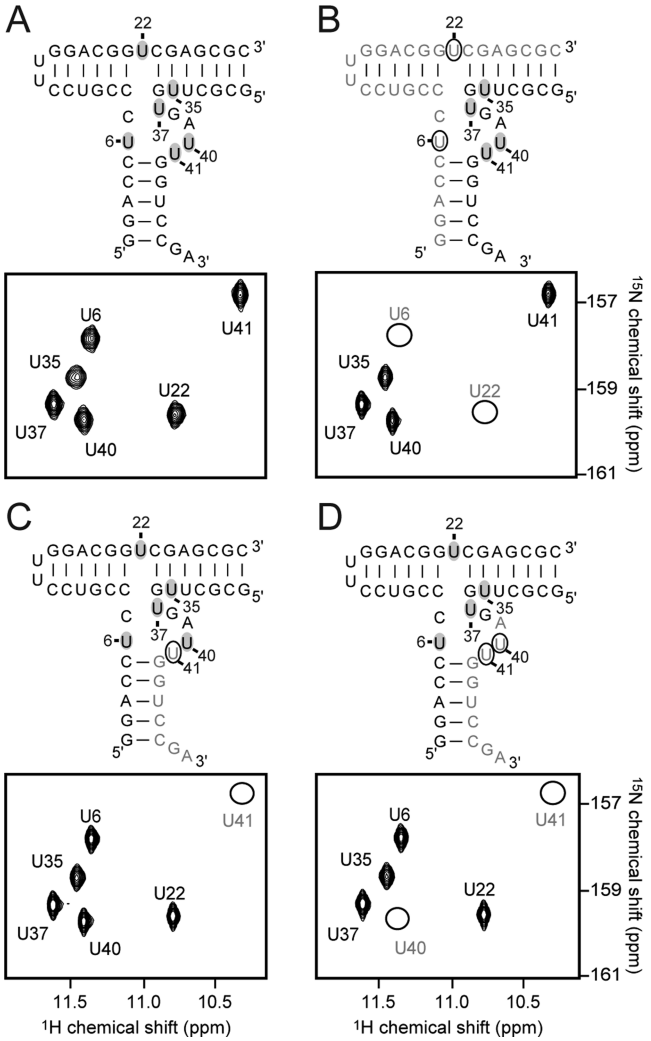

Figure 2. Unambiguous assignment of the uridine imino protons from the core of J345 using ^{15}N segmental labeling. Several complexes similar to the J345 RNA were formed between the S12 and S3 RNAs using different segmental ^{15}N labeling. The sequences and secondary structures of these complexes are shown along with a region of their 2D $^{1}H-^{15}N$ HSQC spectrum: (A) [^{15}N]S12/[^{15}N]S3, (B) unlabeled S12/[^{15}N]S3, (C) [^{15}N]S12/[^{15}N]{30−40}-S3, and (D) [^{15}N]S12/[^{15}N]{30−38}-S3. All RNA complexes are in the presence of 5 mM $MgCl_2$. To illustrate the different ^{15}N labeling schemes, ^{15}N-labeled residues are colored black and unlabeled residues gray. In addition, ^{15}N-labeled and unlabeled uridines from the core are highlighted with gray filled ovals and empty ovals, respectively. Peaks that are absent from the HSQC spectrum are also denoted with empty ovals. The signals of U_{14} and U_{15} are also observed in this region of the spectrum in panels A, C, and D as in Figure 1C but are too weak to appear at the intensity level displayed here.

intestinal alkaline phosphatase (CIP) (Roche Diagnostics) to remove their 5′-phosphates. The unlabeled $S3_{39-48}$ and $S3_{41-48}$ RNAs were chemically synthesized (Thermo Fisher Scientific). The segmentally labeled [^{15}N]{30−38}-S3 and [^{15}N]{30−40}-S3 RNAs (Figure 2) were produced by RNA ligation with the T4 DNA ligase, two S3 fragments, and a single-stranded DNA splint of 19 nucleotides that is fully complementary to S3. Detailed procedures for segmental isotope labeling and preparation of S12/S3 complexes are provided in the Supporting Information. All RNAs were purified by denaturing gel electrophoresis followed by DEAE-Sepharose chromatography.

NMR Sample Preparation. The purified J345 RNAs and the different S12/S3 complexes were concentrated and exchanged in NMR buffer A [10 mM sodium cacodylate (pH 6.5), 50 mM KCl, and 0.05 mM NaN_3] in a 90% H_2O/10% D_2O mixture with Amicon Ultra-4 centrifugation devices (Millipore). The RNAs were then heated at 37 °C for 2 min and cooled in an ice/water mixture for 5 min before the change to the final NMR buffer [NMR buffer A with 5 mM $MgCl_2$ (99.995%) (Sigma-Aldrich)]. For NMR studies in D_2O, the samples were obtained by four cycles of lyophilization and resuspension in 99.996% D_2O.

NMR Spectroscopy. All NMR experiments were conducted on a Varian ^{Unity}INOVA 600 MHz spectrometer equipped with a pulse-field gradient unit and an actively shielded z-gradient $^{1}H/^{13}C/^{15}N$ triple-resonance probe. The resonance assignments and distance restraints were derived from 2D $^{1}H-^{15}N$ HSQC, 2D HNN-COSY, 2D $^{1}H-^{15}N$ CPMG-NOESY, 2D G-specific H(NC)-TOCSY-(C)H, 2D $^{1}H-^{13}C$ CT-HSQC, 2D $^{1}H-^{13}C$ HMQC, 2D $^{1}H-^{15}N$ MQ-(HC)N(C)H, 3D CT-HCCH-COSY, 3D HCCH-TOCSY, 3D ^{15}N-edited NOESY-HSQC, 3D ^{13}C-edited HMQC-NOESY, and 3D $^{15}N/^{13}C$-edited NOESY-HSQC spectra (Tables S1 and S2 of the Supporting Information).[34,54,55] NMR data were processed using the NMRPipe/NMRDraw package[56] and analyzed with the CCPNMR suite.[57]

Structural Restraints. The NOE-derived distance restraints were separated into four classes [strong (1.8−3.3 Å), medium (1.8−4.5 Å), weak (1.8−5.5 Å), and very weak (2.8−8.0 Å)] on the basis of NOE cross-peak intensities. On the basis of NMR evidence from NOESY and HNN-COSY spectra, canonical distance restraints were employed to define the hydrogen bond pattern and planarity of the WC base pairs in helical regions (stem III, 1−5/42−46; SLIV, 8−13/16−21; SLV, 24−27/32−35) as well as the typical G_{28}-A_{31} base pair of the GAAA tetraloop.[58,59] Dihedral-angle restraints for the sugar puckers (δ) and other backbone dihedral angles (α, γ, χ, and ζ) were defined from comparative NOE analyses. On the basis of NMR evidence, backbone torsion angles of residues in helical regions were restrained to A-form values (±15°).

Metal Ion Binding Studies. Manganese (Mn^{2+}) titrations were performed with two J345 samples (1.25 mM ^{15}N-labeled J345 and 2.0 mM ^{13}C- and ^{15}N-labeled J345) in NMR buffer A with 5 mM $MgCl_2$, as previously described.[49] Mn^{2+}-induced paramagnetic relaxation enhancement (PRE) was monitored by 2D $^{1}H-^{15}N$ HSQC[60] spectra at 15 °C and 2D $^{1}H-^{13}C$ CT-HSQC[61,62] spectra at 25 °C.[49] The RNA−metal distance restraints were derived from Mn^{2+}-induced PRE using the ratio of signal intensity (I_o/I_{Mn}) determined from spectra collected at 0 μM $MnCl_2$ (I_o) and 10 μM $MnCl_2$ (I_{Mn}).[49]

Structure Calculation. Three-dimensional structures of J345 were calculated with restrained molecular dynamics and simulated annealing in X-PLOR-NIH version 2.1.9,[63] from structures with randomized backbone angles, as previously described.[55] A force field was used that included bond, angle, improper, and repulsive van der Waals energy terms as well as NOE and torsion-angle pseudoenergy terms. Electrostatic contributions were not included in the force field. Three-dimensional structures of J345 bound to hydrated magnesium complexes [$Mg(H_2O)_n^{2+}$], termed $J345^{Mg}$, were calculated as described for J345 using $Mg(H_2O)_n^{2+}$ coordinates and parameters, as previously described.[49] A pentahydrated Mg^{2+}

dx.doi.org/10.1021/bi500826n | Biochemistry 2014, 53, 6264−6275

Table 1. Structural Statistics for J345 and J345^{Mg}

	J345	J345^{Mg}
no. of experimental restraints		
NOE-derived distance restraints	1780	1780
internucleotide	897	897
intranucleotide	855	855
ambiguous	28	28
hydrogen bond restraints	84	84
base pair planarity restraints	30	30
Mg^{2+}–RNA distance restraints	0	92
dihedral-angle restraints	161	161
total no. of restraints	2055	2147
rmsd from experimental restraints		
NOE (Å) (none >0.2 Å)	0.0088 ± 0.0004	0.0111 ± 0.0002
dihedral (deg) (none >5°)	0.10 ± 0.01	0.11 ± 0.01
rmsd from idealized geometry		
bonds (Å)	0.00368 ± 0.00003	0.00373 ± 0.00003
angles (deg)	0.9969 ± 0.0007	0.9866 ± 0.0007
impropers (deg)	0.392 ± 0.001	0.396 ± 0.002
heavy atom rmsd from the minimized average structure (Å)		
overall (residues 2–45)	3.72 ± 1.62	2.63 ± 0.80
stem III (residues 2–5 and 42–45)	0.35 ± 0.09	0.31 ± 0.08
stem–loop IV (residues 10–19)	0.36 ± 0.09	0.38 ± 0.09
stem–loop V (residues 24–35)	0.82 ± 0.31	0.55 ± 0.18
core domain (residues 6–9, 20–23, and 36–41)	0.97 ± 0.13	1.15 ± 0.16
U_6-U_{41}-C_{23} base triple	0.81 ± 0.19	0.78 ± 0.24
C_7-U_{40}-U_{22} base triple	0.68 ± 0.15	0.86 ± 0.22
C_8-G_{21}-A_{39} base triple	0.46 ± 0.13	0.69 ± 0.18
C_9-G_{20}-G_{38} base triple	0.66 ± 0.25	0.78 ± 0.23

ion $[Mg(H_2O)_5^{2+}]$ was used at site 1 (GAAA tetraloop),[49] whereas sites 2–6 were modeled with hexahydrated Mg^{2+} ions $[Mg(H_2O)_6^{2+}]$. For both J345 and J345^{Mg}, the 20 lowest-energy structures that satisfied all the experimental restraints (all distance violations <0.2 Å and all torsion-angle violations <5°) were selected for analysis and used to calculate an average structure that was minimized against all restraints. Structures were visualized with PyMOL Molecular Graphics System version 1.3 (Schrödinger, LLC) and analyzed with PyMOL and Curves+.[64] Reported values of rmsds, interatomic distances, and interhelical angles are given as average values with standard deviations for the 20 lowest-energy structures, unless otherwise mentioned. Interhelical angles were calculated using residues 1–5 and 42–46 of stem III, residues 8–12 and 17–21 of stem IV, and residues 24–27 and 32–35 of stem V.

RESULTS

The J345 RNA Adopts a Compact Structure in the Presence of Mg^{2+} Ions. The J345 RNA is a 47-nucleotide three-way junction that incorporates all the single-stranded residues of the junction core as well as the proposed proximal base pairs of stems III–V found in the wild-type VS ribozyme (Figure 1A,B).[23] In addition, the J345 RNA contains two non-natural terminal loops that were included to facilitate NMR assignment: a CUUG tetraloop[65] in stem–loop IV and a GAAA tetraloop[58,59] in stem–loop V (Figure 1B). Both tetraloops are closed by a C-G base pair and are termed herein cCUUGg and cGAAAg tetraloops, respectively.

NMR studies of J345 were conducted in the presence of 5 mM $MgCl_2$, because the VS ribozyme requires metal cations, preferentially Mg^{2+} ions, for its folding and catalytic activities.[22−29] Under these conditions, the 2D $^1H-^{15}N$ HSQC spectrum (Figure 1C) is well-dispersed with imino signals representing 24 of the 27 imino groups in J345, in agreement with formation of a unique stable structure for J345. All 24 imino signals were also observed in the absence of Mg^{2+} ions (Figure S1 of the Supporting Information), indicating that addition of Mg^{2+} ions induces only minor changes in the structure of J345. These imino signals could be assigned from NOESY spectra, except for the U imino signals from the junction core.

To allow unambiguous assignment of these U imino signals, a segmental ^{15}N isotope labeling approach was developed using a two-stranded complex similar to J345, designated the S12/S3 complex. The 2D $^1H-^{15}N$ HSQC spectrum of [^{15}N]S12/[^{15}N]S3 (Figure S2 of the Supporting Information) together with 2D HNN-COSY and 3D ^{15}N-edited HSQC-NOESY spectra (not shown) indicates that the S12/S3 complex adopts a structure that is very similar to that of J345. This 2D $^1H-^{15}N$ HSQC spectrum was then compared with that of differentially labeled S12/S3 complexes (Figure 2). The U_6 and U_{22} imino signals disappear with the unlabeled S12/[^{15}N]S3 complex (Figure 2B), the U_{41} imino signal disappears with the [^{15}N]S12/[^{15}N]{30–40}-S3 complex (Figure 2C); whereas the U_{40} and U_{41} imino signals disappear with the [^{15}N]S12/[^{15}N]{30–38}-S3 complex (Figure 2D). The unambiguous assignment of these U imino signals allowed further interpretation of NOESY spectra (Figure S3 of the Supporting Information). Intense NOEs between the U_6 and U_{41} imino protons are consistent with formation of a *cis* WC/WC U_6–U_{41} base pair within the core. In addition, NOE connectivities involving imino protons of four uridines from the core (U_6, U_{22}, U_{40}, and U_{41}) as well as G_{42} and G_{21} from stems III and IV

dx.doi.org/10.1021/bi500826n | *Biochemistry* 2014, 53, 6264–6275

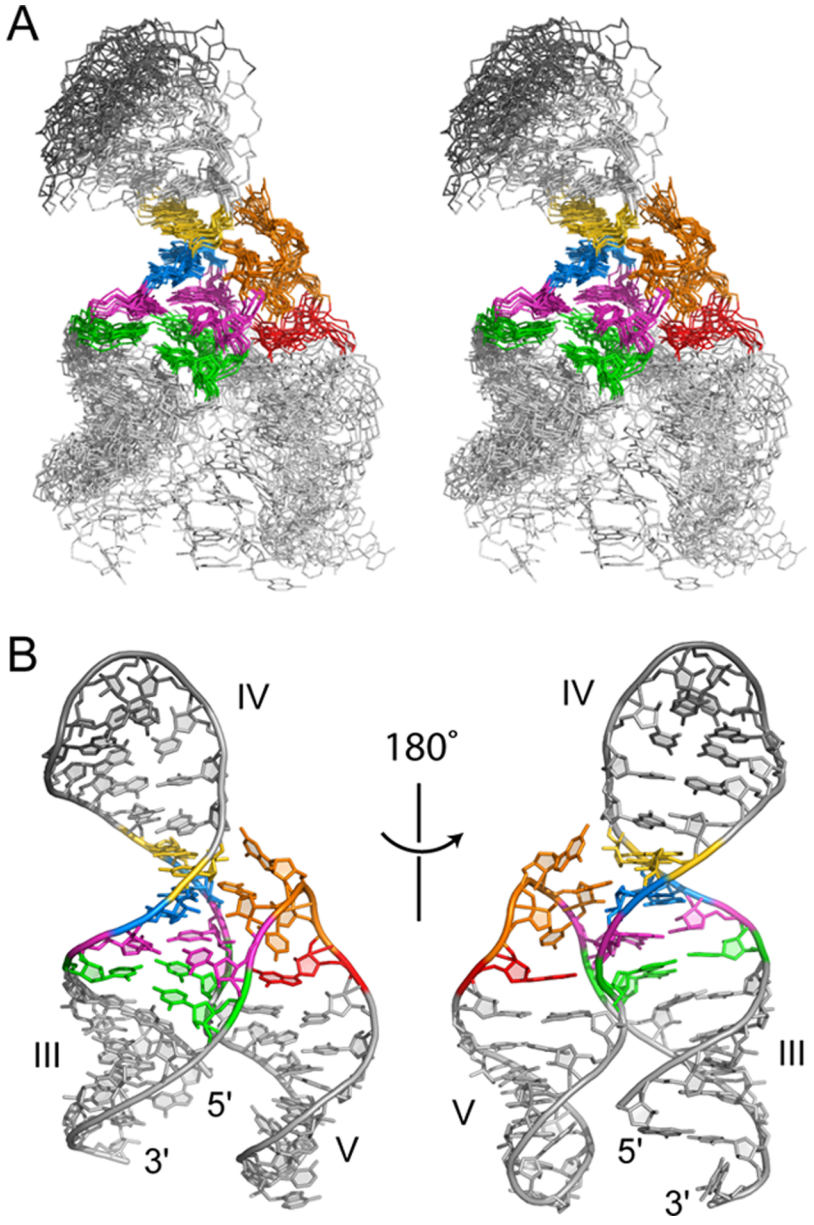

Figure 3. NMR solution structure of the J345 RNA. (A) Stereoview of the 10 lowest-energy structures. Only heavy atoms of core residues (residues 6−9, 20−23, and 36−41) were used for the superposition, but all residues are shown. (B) Stick representations of the minimized average structure of the J345 RNA. In panels A and B, residues are color-coded according to structural elements: the U_6-U_{41}-C_{23} base triple (green), the C_7-U_{40}-U_{22} base triple (magenta), the C_8-G_{21} base pair (blue), the C_9-G_{20} base pair (gold), the U-turn (residues U_{37}, G_{38}, and A_{39}) (orange), G_{36} (red), and the CUUG tetraloop (residues C_{13}−G_{16}) (dark gray).

provide evidence of a highly organized core in which stems III and IV are coaxially stacked, as previously proposed.[1,3,45,48]

Overall NMR Structure of the J345 RNA. The three-dimensional structure of J345 was determined using NOE-derived distance restraints and dihedral-angle restraints. Its overall structure is well-defined by the NMR data with a heavy atom rsmd of 3.72 ± 1.62 Å for the 20 lowest-energy structures (Table 1 and Figure 3). The J345 RNA adopts a Y-shaped fold with a well-defined core domain (rsmd of 0.97 ± 0.13 Å) that orients stem III (rsmd of 0.35 ± 0.09 Å) and stem V (rsmd of 0.82 ± 0.31 Å) side by side and away from stem IV (rsmd of 0.36 ± 0.09 Å). Stems III and V define the most acute interhelical angle (ϕ_{III-V} = 32.8 ± 22.6°), whereas the other two stem pairs define obtuse interhelical angles (ϕ_{IV-V} = 149.3 ± 14.2°, and ϕ_{III-IV} = 167.1 ± 10.1°), with stems III and IV being nearly coaxial.

Compact cCUUGg and cGAAAg Tetraloops Capping Stems IV and V. The $cG_{28}A_{29}A_{30}A_{31}g$ tetraloop in stem−loop V adopts a typical GNRA fold,[58,59] with a *cis* WC/WC C-G closing base pair (C_{27}-G_{32}), a *trans* sugar edge/Hoogsteen G-A base pair between the first and last residues of the loop (G_{28}-A_{31}), a sharp backbone turn between the first and second residues (G_{28} and A_{29}), 3′-stacking among the last three bases of the loop, and two typical hydrogen bonds (not shown). In contrast, the cCUUGg tetraloop adopts a structure different from that previously reported for the related gCUUGc tetraloop.[65] In J345, the $cC_{13}U_{14}U_{15}G_{16}g$ tetraloop is stabilized by two *cis* WC/WC C-G base pairs: the C_{12}-G_{17} closing base pair and the C_{13}-G_{16} base pair between the first and last

dx.doi.org/10.1021/bi500826n | *Biochemistry* 2014, 53, 6264−6275

residues of the loop (Figure 4). An analysis of rotamer geometries yields non-A-form values for residues U_{14}, U_{15}, and

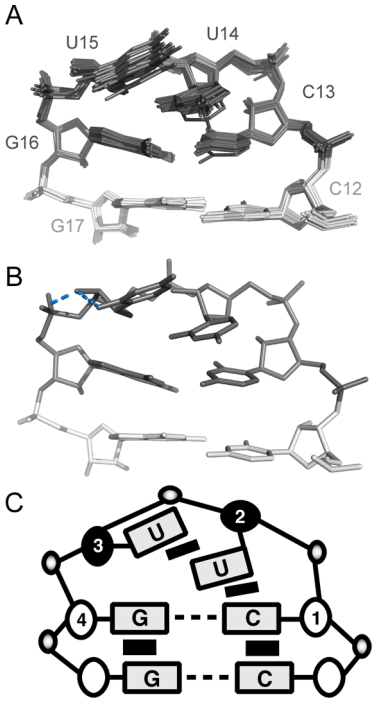

Figure 4. cCUUGg tetraloop of the J345 RNA. (A) Superposition of the 20 lowest-energy structures. Only heavy atoms of residues 12−17 were used for the superposition and are shown. (B) Stick representation of the lowest-energy structure of the cCUUGg tetraloop. Cyan dashed lines represent hydrogen bonds that are defined on the basis of short distances between heavy atoms in the ensemble of structures: U_{15} O2′ and the 5′-phosphate oxygen of G_{16} (2.51 ± 0.27 Å) and U_{15} O2′ and U_{15} O2 (2.82 ± 0.05 Å). In panels A and B, the CUUG residues are colored dark gray whereas those forming the closing base pair (C_{12} and G_{17}) are colored light gray. (C) Schematic representation of the cCUUGg loop. The light gray boxes represent the bases, the large ovals the riboses in a C2′-*endo* (filled) or C3′-*endo* (empty) conformation, and the small ovals the phosphates. Dashed lines denote WC base pairs, and black rectangles indicate base stacking interactions.

G_{16},[66] in agreement with the backbone turn of this cCUUGg tetraloop not being as sharp as that of the GNRA tetraloop (Figure 4). In addition, the cCUUGg tetraloop displays 5′-stacking among the first three bases of the loop [C_{13}, U_{14}, and U_{15} (Figure 4)]. All the residues in the cCUUGg tetraloop have glycosidic angles in the *anti* conformation and sugar puckers in the C3′-*endo* conformation, with the exception of U_{14} and U_{15} that adopt a C2′-*endo* sugar pucker. There are two hydrogen bonds that potentially stabilize the cCUUGg loop as evidenced by short interatomic distances involving U_{15} O2′ (Figure 4B). In summary, the cCUUGg tetraloop bears a structural resemblance to the cGAAAg tetraloop with respect to the formation of base pairing, hydrogen bonding, and stacking interactions, but there are significant differences in terms of the residues involved in these interactions and the backbone geometry.

Formation of a U-Turn at the Junction Core. As proposed previously,[46] residues U_{37}, G_{38}, and A_{39} adopt a canonical U-turn structure within the well-defined core domain of J345 (Figure 5).[67] In the J345 structure, the U-turn stacks on stem V and produces a sharp turn in the backbone after U_{37} that positions stem V side by side with respect to stem III. In addition, two hydrogen bonds, typical of the U-turn fold, are observed between U_{37} 2′-OH and A_{39} N7 and between U_{37} H3 and A_{39} 3′-phosphate (Figure 5B).

The G_{36} residue preceding the U-turn does not form a canonical *cis* WC/WC base pair with C_{23}, as previously proposed.[23] Rather, G_{36} forms a cross-strand hydrogen bond involving its amino group and the phosphate of C_{23} [G_{36} N2−C_{23} 5′-phosphate oxygen distance of 3.40 ± 0.50 Å (Figure 5)], while the C_{23} base is flipped out to fulfill other interactions within the core. These cross-strand interactions involving G_{36} likely stabilize the U-turn by allowing continuous stacking among U_{37}, G_{36}, and the G_{24}-U_{35} base pair.

A Complex Network of Interactions within the Core of the III−IV−V Junction. The core domain of J345 is stabilized by a stack of four base triples that is well-defined by the NMR data (Figures 5 and 6). Within the U_6-U_{41}-C_{23} base triple (rmsd of 0.81 ± 0.19 Å), U_6 and U_{41} form a *cis* WC/WC U-U base pair, and the major groove of this U_6-U_{41} base pair interacts with the flipped-out base of C_{23} through a single hydrogen bond. The U_6-U_{41}-C_{23} base triple stacks on the C_7-U_{40}-U_{22} base triple (rmsd of 0.68 ± 0.15 Å), which is stabilized by three hydrogen bonds involving the WC edges of these residues. The C_7-U_{40}-U_{22} base triple stacks on the C_8-G_{21}-A_{39} base triple (rmsd of 0.46 ± 0.13 Å), where C_8 and G_{21} form a canonical *cis* WC/WC base pair at the end of stem IV, while A_{39} of the U-turn participates in a type I A-minor interaction with the C_8-G_{21} base pair.[9] Finally, the C_8-G_{21}-A_{39} base triple stacks on the C_9-G_{20}-G_{38} base triple (rmsd of 0.66 ± 0.25 Å), where C_9 and G_{20} form a canonical *cis* WC/WC base pair in stem IV, while G_{38} interacts with the minor groove of the C_9-G_{20} base pair. Although the base of G_{38} is not well-defined in the ensemble of NMR structures (Figure 5), G_{38} could potentially form several hydrogen bonds with the riboses of C_9 (Figure 6) and G_{10} [G_{38} NH_2 to G_{10} O4′ and O2′ (not shown)].

The stack of four base triples within the J345 core is also stabilized by a ribose zipper,[10] which involves close backbone contacts of G_{38} and A_{39} from the U-turn with C_8 and C_9 of stem IV. As is typical of ribose zippers,[10] several hydrogen bonds are observed that involve consecutive 2′-OH groups (Figure S4 of the Supporting Information). Such a network of interactions allows close packing of the U-turn within the junction core.

Identification of $Mg(H_2O)_n^{2+}$-Binding Sites. The structure of J345 in complex with $Mg(H_2O)_n^{2+}$ ($J345^{Mg}$) was determined by adding metal−RNA restraints derived from Mn^{2+}-induced PRE to the existing set of experimental restraints (Table 1 and Table S3 of the Supporting Information). The overall structure of the $J345^{Mg}$ RNA is very well-defined by the NMR data with a heavy atom rmsd of 2.63 ± 0.80 Å (Table 1). In comparison with J345, the global structure of $J345^{Mg}$ is better defined, even though local structural elements have similar resolutions in both structures.

The $J345^{Mg}$ structure displays six Mg^{2+}-binding sites (Figure 7A), and potential metal ligands at these sites were defined on the basis of distance measurements (Table S4 of the Supporting Information). These sites defined by the NMR data should be viewed as preferential sites for Mg^{2+} ion binding, and no inference can be made in terms of the occupancy of the metal at a given site. The $Mg(H_2O)_5^{2+}$ at site 1 is associated with the $cG_{28}A_{29}A_{30}A_{31}g$ tetraloop, whereas the $Mg(H_2O)_6^{2+}$ species at sites 2 and 4 are associated with the major grooves of stems V and IV, respectively (Figure S5A−C of the Supporting Information), in agreement with previous observations.[49] The

dx.doi.org/10.1021/bi500826n | *Biochemistry* 2014, 53, 6264−6275

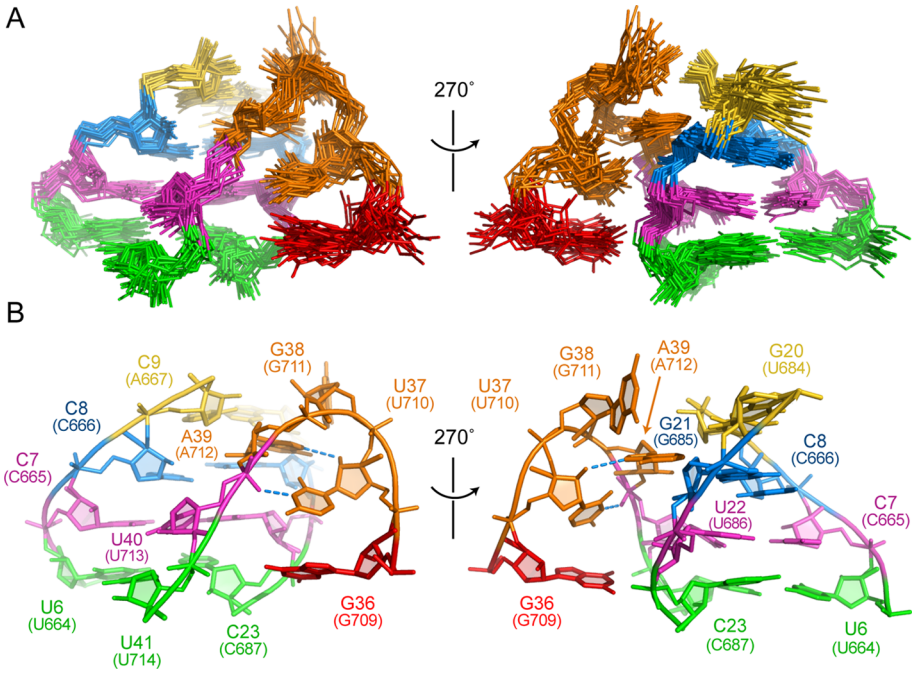

Figure 5. NMR structure of the core domain of the J345 RNA. (A) Superposition of the 20 lowest-energy structures. Only heavy atoms of core residues (6–9, 20–23, and 36–41) were used for the superposition and are shown. (B) Stick representations of the lowest-energy structure of the core domain. The cyan dashed lines represent characteristic hydrogen bonds of the U-turn motif that are defined on the basis of short distances between heavy atoms in the ensemble of structures: U_{37} O2′ to A_{39} N7 (3.12 ± 0.44 Å) and U_{37} N3 to A_{39} 3′-phosphate oxygen (19 of 20 structures, 3.08 ± 0.56 Å).

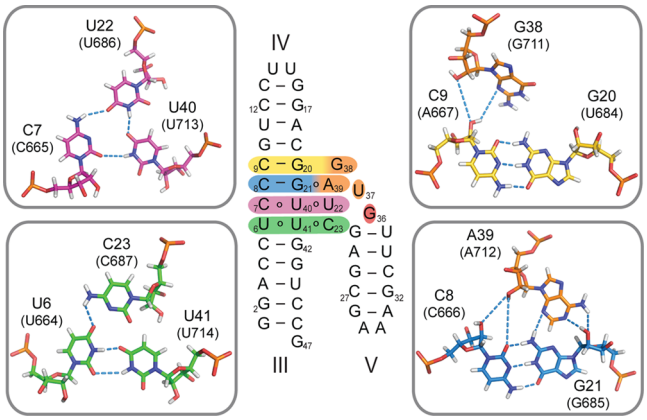

Figure 6. Base triples within the core domain of the J345 RNA. The four base triples are located on the secondary structure of J345 derived from the NMR structure (center), and their hydrogen bonding pattern is shown on the lowest-energy structure (sides). Cyan dashed lines represent hydrogen bonds that are defined on the basis of short distances (≥4.0 Å) between heavy atoms observed in the ensemble of structures.

$Mg(H_2O)_6^{2+}$ at site 3 is associated with the cCUUGg tetraloop (Figure 7B). The O6 and N7 atoms of G_{16} and G_{17} act as potential outer-sphere ligands, whereas the G_{16} 5′-PO_4^- contributes to electrostatic stabilization of the Mg^{2+} ion. The $Mg(H_2O)_6^{2+}$ at site 5 is associated with the minor groove of the U-turn within the core domain (Figure 7C), where the ribose phosphate of the U-turn (residues 37–40) provides several outer-sphere ligands as well as electrostatic stabilization. Remarkably, a cation–π interaction is also observed between this $Mg(H_2O)_6^{2+}$ and the U_{37} base that defines the U-turn. The Mg^{2+} ion at this position is likely important for stabilization of the U-turn fold. The $Mg(H_2O)_6^{2+}$ at site 6 is located near the U_6-U_{41}-C_{23} base triple of the core domain within a pocket formed by the major groove of stem III and the phosphate backbone of stem V (Figure 7D). Residues C_{23}, G_{24}, G_{42}, and G_{43} provide several potential ligands, whereas the 5′-phosphates of G_{24} and G_{42} contribute to electrostatic stabilization of the Mg^{2+} ion. Site 6 is unique in that Mn^{2+}-induced PRE affects residues of both stems III and V (Table S3 of the Supporting Information). Thus, RNA–metal restraints at this site help improve the overall rmsd of J345 by better defining the relative orientation of these two stems.

DISCUSSION

As part of our quest to understand the structural basis for substrate recognition and cleavage by the VS ribozyme, we determined the high-resolution solution structure of J345, which contains a three-way junction that plays a key role in defining the global architecture of the VS ribozyme. In addition, we localized Mg^{2+}-binding sites within J345 using Mn^{2+}-induced PRE. The structure of J345 reveals an intricate network of interactions at the junction core as well as a novel fold for the cCUUGg tetraloop that was introduced to stabilize stem–loop IV, and both are discussed below in light of previous studies.

A Novel cCUUGg Tetraloop Structure. To date, thermodynamic and structural studies of CUUG tetraloops have mostly focused on the gCUUGc sequence because of its greater prevalence in rRNA.[68,69] The gCUUGc and cCUUGg tetraloops are considered unusually stable tetraloops,[70] although they are less stable than the more common cGNRAg and cUNCGg tetraloops.[71,72] At this time, symbolic searches within the nonredundant list of RNA-containing structures from the Protein Data Bank (PDB) using WebFR3D[73] revealed two essentially identical structures of gCUUGc tetraloops, one from the NMR structure of a short RNA hairpin (PDB entry 1RNG)[65] and one from the X-ray structure of the *Escherichia*

dx.doi.org/10.1021/bi500826n | *Biochemistry* 2014, 53, 6264–6275

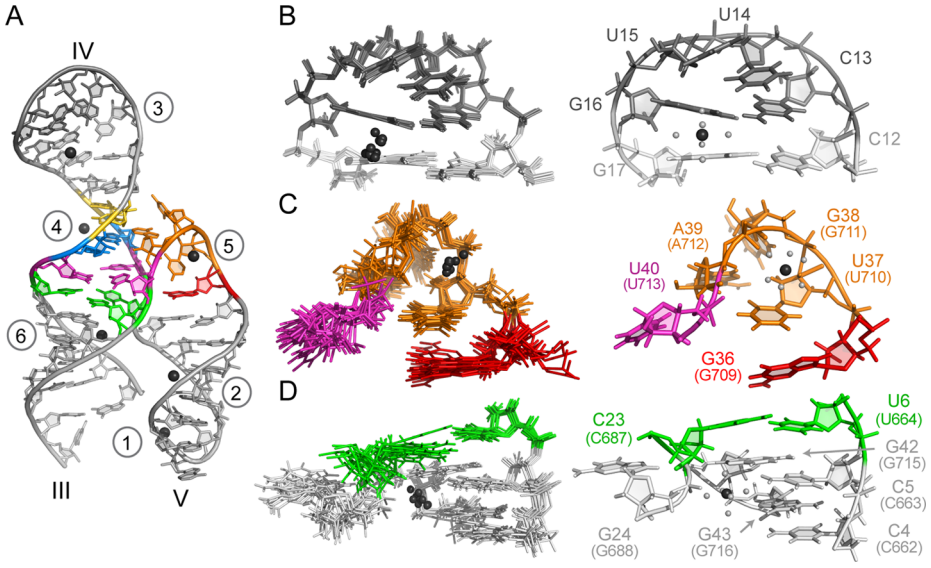

Figure 7. $Mg(H_2O)_n^{2+}$-binding sites within the $J345^{Mg}$ RNA. (A) Stick representation of the lowest-energy structure of $J345^{Mg}$ with the six metal-binding sites, numbered 1–6. (B–D) $Mg(H_2O)_6^{2+}$-binding sites associated with (B) the cCUUGg tetraloop (site 3; in 20 of 20 structures), (C) the major groove face of the U-turn (site 5; in 16 of 20 structures), and (D) the core domain (site 6; in 20 of 20 structures). For each $Mg(H_2O)_6^{2+}$-binding site, the heavy atom superposition of the 10 lowest-energy structures is shown (left panels; only the residues shown were used for the superposition) along with a stick representation of the lowest-energy structure (right panels). The Mg^{2+} ions are colored black, with their bound water molecules colored dark gray.

coli ribosome (PDB entry 2AW7);[74] however, there is no available structure for the cCUUGg loop.

The NMR structure of J345 reveals that the cCUUGg tetraloop structure is significantly different from those reported for the gCUUGc tetraloop, in agreement with previous circular dichroism studies.[70] One important characteristic of the gCUUGc structures is that the first uridine is extruded into the minor groove, forming hydrogen bonds with the closing and loop base pairs.[65,74] In contrast, the cCUUGg tetraloop adopts a compact fold with consecutive stacking of the first three residues. This main structural difference may arise from the inversion of the closing base pair (G-C to C-G), which does not allow hydrogen bonding of an extruded U residue in the minor groove in the cCUUGg tetraloop.[65,74] This structural difference could also be due to the presence of Mg^{2+} ions in our study, because the NMR structure of the gCUUGc tetraloop was determined in the absence of Mg^{2+} ions.[65] Using Mn^{2+}-induced PRE, we identified a Mg^{2+}-binding site associated with the major groove of the cCUUGg tetraloop that likely helps stabilize the observed fold.

An important feature of the cCUUGg tetraloop is that the WC edges of the loop residues are all oriented toward the major groove. In contrast, both the GNRA and gCUUGc tetraloops expose loop bases in the minor groove. In the GNRA tetraloop, these bases are known to play important roles in forming tertiary interactions.[75,76] Although the gCUUGc tetraloop is free in the context of the folded *E. coli* ribosome,[74] protrusion of its first uridine into the minor groove could allow for RNA–RNA or RNA–protein interactions in other contexts.[65] In contrast, the exposed bases of the cCUUGg tetraloop appear to be more retracted in the major groove and less accessible for tertiary contacts, and this may explain the low frequency of this tetraloop in rRNA.

Compatibility of the J345 Structure with Biochemical Data. The NMR structure of J345 reveals a complex network of interactions for the VS ribozyme III–IV–V junction that is in agreement with previous biochemical data. The NMR structure clearly demonstrates that residues U_{710}, G_{711}, and A_{712} adopt a canonical U-turn structure (Figure 5), in agreement with its functional substitution with a hairpin, as well as mutational and chemical probing data.[23,24,26,28,29,38,45,46] In particular, the effect of base substitutions on both cleavage and ligation activities is in agreement with the UNR consensus sequence (N is any base, and R is A or G) of the U-turn.[38,45,46] Furthermore, the specific requirement for an adenine at the R position is in agreement with the observed A-minor interaction involving A_{712} (Figure 6).

Kinetic studies of VS ribozyme variants carrying single-nucleotide substitutions have previously highlighted the importance of several residues in and around the junction.[38,45,46] For the sake of simplicity, we restrict our discussion to the effect of base substitutions on cleavage activity of the VS ribozyme;[45,46] however, similar effects on its ligation activity were also observed.[38] In particular, base substitutions of all junction residues initially predicted to be single-stranded (Figure 1A) reduced cleavage activity, except for G_{711}.[45,46] This is in agreement with the NMR structure of J345 in which all bases within the junction core are directly involved in stable hydrogen bonding and stacking interactions (Figures 5 and 6), except for the less-well-defined G_{711} (G_{38}) that likely forms less stable interactions. In terms of the junction proximal base pairs, only a 4-fold reduction in cleavage activity was observed for inversion of the closing base pair of stem III (C_{663}-G_{715}), whereas inversion of the proposed closing base pairs of stem IV (C_{666}-G_{685}) and stem V (C_{687}-G_{709}) reduced the VS ribozyme cleavage activity by 30- and 125-fold, respectively.[45] These results are consistent with the C_{666}-G_{685} base pair forming a base triple with A_{712} (Figure 6) and with the previously proposed C_{687}-G_{709} base pair (Figure 1A,B) not being present in the J345 structure determined here.[23] Rather, C_{687} forms a base triple (U_{664}-U_{714}-C_{687}), and G_{709} forms cross-strand stacking and hydrogen bonding interactions (Figures 5 and 6).

dx.doi.org/10.1021/bi500826n | *Biochemistry* 2014, 53, 6264–6275

Chemical probing experiments conducted in the presence of Mg^{2+} ions are also in agreement with the NMR structure of J345. The WC edges of all the junction residues initially predicted to be single-stranded are protected from chemical modifications under native conditions, with the exception of G_{711} (G_{38}),[23,28,29] in agreement with the J345 structure. In addition, chemical modifications of bases that play an important role in the structure of the III−IV−V junction have been shown to significantly interfere with self-cleavage; this includes carboxyethylation at the N7 position of G_{709} (G_{36}) and A_{712} (A_{39}) by diethyl pyrocarbonate (DEPC) and removal of U_{686} (U_{22}) and U_{710} (U_{37}) by hydrazine.[24] The involvement of A_{712} in the U-turn and A-minor interaction (Figures 5 and 6) also helps explain results of adenine analogue interference experiments, in which chemical modifications at the N7 and C2 positions significantly inhibit cleavage activity.[37,77] Considering the backbone, the 5′-phosphates of A_{712} (A_{39}) and U_{713} (U_{40}) are protected from ethylnitrosourea modifications,[26] which is supported by Mg^{2+} binding (Figure 7) and hydrogen bonding within the U-turn (Figure 5B). In addition, C_{666} (C_8), A_{667} (C_9), U_{686} (U_{22}), C_{687} (C_{23}), and A_{712} (A_{39}) are protected from hydroxyl radical footprinting,[27] consistent with the poor accessibility of their C4′ atoms within the ribose zipper [for C_{666}, A_{667}, and A_{712} (Figure S4 of the Supporting Information)] and base triples [for U_{686}, C_{687}, and A_{712} (Figure 6)]. Moreover, 2′-deoxynucleotide modifications of several residues in the III−IV−V junction (C_{666}, U_{686}, U_{710}, A_{712}, and U_{713}) were shown to significantly inhibit the cleavage and/or ligation activities of the VS ribozyme, in agreement with the importance of these 2′-hydroxyls in the ribose zipper (Figure S4 of the Supporting Information), the U-turn (Figure 5), and several base triples (Figure 6).[37,78] Hence, the NMR structure of J345 is consistent with previous biochemical data and most likely represents the conformation of the III−IV−V junction in the context of the active VS ribozyme.

The Topology of the III−IV−V Junction Is Typical of Family C Three-Way Junctions. The NMR structure of J345 confirms that the III−IV−V junction of the VS ribozyme adopts a global Y-shaped fold typical of family C three-way junctions, as previously proposed.[1,3] Previous predictions also indicated two potential coaxial stacking interactions, either between stems IV and V[47] or between stems III and IV.[1,3] The NMR structure establishes that stems III and IV are coaxially stacked and that there is an acute angle between stems III and V. This coaxial stacking of stems III and IV is also in agreement with low-resolution structural models based on FRET and SAXS data.[45,48] Although these models could not precisely account for the structural complexity of the III−IV−V junction, they both predicted an acute interhelical angle between stems III and V (ϕ_{III-V}).[45,48] Interestingly, the ϕ_{III-V} value of ∼40° estimated from the SAXS model[48] falls within the range observed in the ensemble of NMR structures of J345 (ϕ_{III-V} = 32.8 ± 22.6°).

Diverse Roles for Three-Way Junctions in Long-Range Tertiary Interactions. The structure of the III−IV−V junction relies on numerous local structural elements that have been previously found in several family C three-way junctions, namely, a U-turn motif, noncanonical base pairs, and base triples, the formation of A-minor and cross-strand interactions, and a ribose zipper.[1,5−8,79−90] However, the III−IV−V junction does not include a long-range interaction between the helices that are positioned side by side (stems III and V),[2] as commonly found in family C three-way junctions from various RNAs.[1,5,7,8,79−90] Instead, the III−IV−V junction of the VS ribozyme allows for the interaction between SLV and an exogenous stem−loop (SLI) that does not contribute to forming the junction,[30−34] and to the best of our knowledge, this type of tertiary interaction for family C three-way junctions has not been previously reported. Thus, this study expands on our understanding of the diverse roles that three-way junctions play in the organization of complex RNA structures, which could have useful applications in nanotechnologies.

Effect of Mg^{2+} Ions on the Folding of the III−IV−V Junction. Chemical probing data of the VS ribozyme have shown increased levels of protection of several residues of the junction upon addition of Mg^{2+} ions.[23,24,26−29] In addition, native gel and FRET studies have provided evidence of a Mg^{2+}-induced structural transition that alters the global structure of the III−IV−V junction.[45] From these studies, it was proposed that the junction adopts an extended structure in the absence of divalent metal ions that folds upon addition of Mg^{2+} ions.[45] However, the NMR data of J345 presented here indicate that the III−IV−V junction is prefolded in the absence of divalent cations and that the local structural features of the junction are not considerably altered upon addition of Mg^{2+} ions. Moreover, the presence of two divalent metal-binding sites in the core of the III−IV−V junction indicates that these divalent cations help stabilize both the U-turn motif and the close packing of stems III and V. This is in agreement with results from FRET studies in which an increasing Mg^{2+} ion concentration systematically reduced the end-to-end distance between stems III and V.[45] Taken together, these data support a model in which Mg^{2+} ion binding helps stabilize a preformed structure at the III−IV−V junction to allow close packing of stems III and V.

The III−IV−V Junction Forms a Dynamic Hinge for SLI Substrate Recognition and Catalysis. The main role of the III−IV−V junction in the VS ribozyme is to properly orient SLV for SLI substrate binding and catalysis. As currently viewed, SLV forms a high-affinity kissing loop interaction with SLI,[33] and this facilitates the association between the SLI and SLVI internal loops to form the active site. With this study, we establish that SLV is not locked by tertiary interactions with SLIII as would be expected for a typical family C three-way junction. Rather, SLV appears to have a certain degree of flexibility with respect to SLIII, and thus, the junction most likely functions as a dynamic hinge to assist SLV in exploring the conformational space needed to facilitate SLI binding and catalysis. In particular, a certain degree of flexibility may be required to allow formation of the active site through the intimate association of the SLI and SLVI internal loops.

■ ASSOCIATED CONTENT

Supporting Information

Experimental procedures providing more details about the methods used in this study; figures that show NMR evidence that J345 adopts a single stable structure in the absence of Mg^{2+} ions that is similar to that formed in the presence of Mg^{2+} ions (Figure S1), NMR evidence that the S12/S3 complex adopts a structure similar to that of J345 (Figure S2), NMR evidence that J345 forms a highly organized core with helical stacking between stems III and IV (Figure S3), a representation of the ribose zipper within the core domain of the J345 RNA (Figure S4), and representations of additional $Mg(H_2O)_n^{2+}$-binding sites within $J345^{Mg}$ (Figure S5); and tables that show the resonance assignment of J345 (Tables S1 and S2), distance restraints derived from Mn^{2+}-induced PRE used for the $J345^{Mg}$

dx.doi.org/10.1021/bi500826n | Biochemistry 2014, 53, 6264−6275

structure calculation (Table S3), and structural characteristics of $Mg(H_2O)_n^{2+}$-binding sites in $J345^{Mg}$ (Table S4). This material is available free of charge via the Internet at http://pubs.acs.org.

Accession Codes

NMR chemical shifts, structural restraints, and structural coordinates have been deposited for J345 and $J345^{Mg}$ as BMRB entries 25163 and 25164 and PDB entries 2mtj and 2mtk, respectively.

AUTHOR INFORMATION

Corresponding Author

*E-mail: pascale.legault@umontreal.ca. Phone: (514) 343-7326. Fax: (514) 343-2210.

Funding

This work was supported by the Canadian Institutes of Health Research (CIHR) (Grant MOP-86502 to P.L.). E.B. was supported by a Frederick Banting and Charles Best Canada Graduate Scholarship Ph.D. scholarship from CIHR and graduate scholarships from the Université de Montréal. P.L. holds a Canada Research Chair in Structural Biology and Engineering of RNA. Funding for open access charge provided by CIHR.

Notes

The authors declare no competing financial interest.

ACKNOWLEDGMENTS

We thank Thomas R. Cech for providing the expression vector for the T4 DNA ligase, Mathieu Lussier-Price for help with the purification of the T4 DNA ligase, Dominique Chaussé for help with sample preparation, and Ryan Richter for providing computer scripts for structural analysis and for computer support. We also thank Nicolas Girard, Patricia Bouchard, and James G. Omichinski for discussions and critical reading of the manuscript.

ABBREVIATIONS

2D, two-dimensional; 3D, three-dimensional; FRET, fluorescence resonance energy transfer; HNN-COSY, HNN-correlated spectroscopy; HSQC, heteronuclear single-quantum coherence; Mg^{2+}, magnesium ion; Mn^{2+}, manganese ion; NOE, nuclear Overhauser effect; NOESY, NOE spectroscopy; PDB, Protein Data Bank; PRE, paramagnetic relaxation enhancement; SLI, stem−loop I; SLII, stem−loop II; SLV, stem−loop V; SLVI, stem−loop VI; rmsd, root-mean-square deviation; SAXS, small-angle X-ray scattering; VS, Varkud satellite; WC, Watson−Crick.

REFERENCES

(1) Lescoute, A., and Westhof, E. (2006) Topology of three-way junctions in folded RNAs. *RNA 12*, 83−93.

(2) de la Pena, M., Dufour, D., and Gallego, J. (2009) Three-way RNA junctions with remote tertiary contacts: A recurrent and highly versatile fold. *RNA 15*, 1949−1964.

(3) Laing, C., Wen, D., Wang, J. T., and Schlick, T. (2012) Predicting coaxial helical stacking in RNA junctions. *Nucleic Acids Res. 40*, 487−498.

(4) Woodson, S. A., and Leontis, N. B. (1998) Structure and dynamics of ribosomal RNA. *Curr. Opin. Struct. Biol. 8*, 294−300.

(5) Batey, R. T., Gilbert, S. D., and Montange, R. K. (2004) Structure of a natural guanine-responsive riboswitch complexed with the metabolite hypoxanthine. *Nature 432*, 411−415.

(6) Serganov, A., Yuan, Y. R., Pikovskaya, O., Polonskaia, A., Malinina, L., Phan, A. T., Hobartner, C., Micura, R., Breaker, R. R., and Patel, D. J. (2004) Structural basis for discriminative regulation of gene expression by adenine- and guanine-sensing mRNAs. *Chem. Biol. 11*, 1729−1741.

(7) Cate, J. H., Gooding, A. R., Podell, E., Zhou, K., Golden, B. L., Kundrot, C. E., Cech, T. R., and Doudna, J. A. (1996) Crystal structure of a group I ribozyme domain: Principles of RNA packing. *Science 273*, 1678−1685.

(8) Krasilnikov, A. S., Yang, X., Pan, T., and Mondragon, A. (2003) Crystal structure of the specificity domain of ribonuclease P. *Nature 421*, 760−764.

(9) Nissen, P., Ippolito, J. A., Ban, N., Moore, P. B., and Steitz, T. A. (2001) RNA tertiary interaction in the large ribosomal subunit: The A-minor motif. *Proc. Natl. Acad. Sci. U.S.A. 98*, 4899−4903.

(10) Tamura, M., and Holbrook, S. R. (2002) Sequence and structural conservation in RNA ribose zippers. *J. Mol. Biol. 320*, 455−474.

(11) Draper, D. E. (2004) A guide to ions and RNA structure. *RNA 10*, 335−343.

(12) Wakeman, C. A., Ramesh, A., and Winkler, W. C. (2009) Multiple metal-binding cores are required for metalloregulation by M-box riboswitch RNAs. *J. Mol. Biol. 392*, 723−735.

(13) Chen, G., Tan, Z. J., and Chen, S. J. (2010) Salt-dependent folding energy landscape of RNA three-way junction. *Biophys. J. 98*, 111−120.

(14) Zhang, H., Endrizzi, J. A., Shu, Y., Haque, F., Sauter, C., Shlyakhtenko, L. S., Lyubchenko, Y., Guo, P., and Chi, Y. I. (2013) Crystal structure of 3WJ core revealing divalent ion-promoted thermostability and assembly of the Phi29 hexameric motor pRNA. *RNA 19*, 1226−1237.

(15) Saville, B. J., and Collins, R. A. (1990) A site-specific self-cleavage reaction performed by a novel RNA in *Neurospora* mitochondria. *Cell 61*, 685−696.

(16) Collins, R. A. (2002) The *Neurospora* Varkud satellite ribozyme. *Biochem. Soc. Trans. Rev. 30*, 1122−1126.

(17) Lilley, D. M. (2004) The Varkud satellite ribozyme. *RNA 10*, 151−158.

(18) Lilley, D. M. J. (2008) The hairpin and Varkud satellite ribozymes. In *Ribozymes and RNA catalysis* (Lilley, D. M. J., and Eckstein, F., Eds.) pp 66−91, Royal Society of Chemistry, Cambridge, U.K.

(19) Cochrane, J. C., and Strobel, S. A. (2008) Catalytic strategies of self-cleaving ribozymes. *Acc. Chem. Res. 41*, 1027−1035.

(20) Wilson, T. J., and Lilley, D. M. (2011) Do the hairpin and VS ribozymes share a common catalytic mechanism based on general acid-base catalysis? A critical assessment of available experimental data. *RNA 17*, 213−221.

(21) Saville, B. L., and Collins, R. A. (1991) RNA-mediated ligation of self-cleavage products of a *Neurospora* mitochondrial plasmid transcript. *Proc. Natl. Acad. Sci. U.S.A. 88*, 8826−8830.

(22) Collins, R. A., and Olive, J. E. (1993) Reaction conditions and kinetics of self-cleavage of a ribozyme derived from *Neurospora* VS RNA. *Biochemistry 32*, 2795−2799.

(23) Beattie, T. L., Olive, J. E., and Collins, R. A. (1995) A secondary-structure model for the self-cleaving region of *Neurospora* VS RNA. *Proc. Natl. Acad. Sci. U.S.A. 92*, 4686−4690.

(24) Beattie, T. L., and Collins, R. A. (1997) Identification of functional domains in the self-cleaving *Neurospora* VS ribozyme using damage selection. *J. Mol. Biol. 267*, 830−840.

(25) Murray, J. B., Seyhan, A. A., Walter, N. G., Burke, J. M., and Scott, W. G. (1998) The hammerhead, hairpin and VS ribozymes are catalytically proficient in monovalent cations alone. *Chem. Biol. 5*, 587−595.

(26) Sood, V. D., Beattie, T. L., and Collins, R. A. (1998) Identification of phosphate groups involved in metal binding and tertiary interactions in the core of the *Neurospora* VS ribozyme. *J. Mol. Biol. 282*, 741−750.

(27) Hiley, S. L., and Collins, R. A. (2001) Rapid formation of a solvent-inaccessible core in the *Neurospora* Varkud satellite ribozyme. *EMBO J. 20*, 5461−5469.
(28) Sood, V. D., and Collins, R. A. (2002) Identification of the catalytic subdomain of the VS ribozyme and evidence for remarkable sequence tolerance in the active site loop. *J. Mol. Biol. 320*, 443−454.
(29) Maguire, J. L., and Collins, R. A. (2001) Effects of cobalt hexammine on folding and self-cleavage of the *Neurospora* VS ribozyme. *J. Mol. Biol. 309*, 45−56.
(30) Rastogi, T., Beattie, T. L., Olive, J. E., and Collins, R. A. (1996) A long-range pseudoknot is required for activity of the *Neurospora* VS ribozyme. *EMBO J. 15*, 2820−2825.
(31) Andersen, A., and Collins, R. A. (2000) Rearrangement of a stable RNA secondary structure during VS ribozyme catalysis. *Mol. Cell 5*, 469−478.
(32) Andersen, A. A., and Collins, R. A. (2001) Intramolecular secondary structure rearrangement by the kissing interaction of the *Neurospora* VS ribozyme. *Proc. Natl. Acad. Sci. U.S.A. 98*, 7730−7735.
(33) Bouchard, P., and Legault, P. (2014) A remarkably stable kissing-loop interaction defines substrate recognition by the *Neurospora* Varkud Satellite ribozyme. *RNA 20*, 1451−1464.
(34) Bouchard, P., and Legault, P. (2014) Structural insights into substrate recognition by the *Neurospora* Varkud satellite ribozyme: Importance of U-turns at the kissing-loop junction. *Biochemistry 53*, 258−269.
(35) Wilson, T. J., McLeod, A. C., and Lilley, D. M. (2007) A guanine nucleobase important for catalysis by the VS ribozyme. *EMBO J. 26*, 2489−2500.
(36) Desjardins, G., Bonneau, E., Girard, N., Boisbouvier, J., and Legault, P. (2011) NMR structure of the A730 loop of the *Neurospora* VS ribozyme: Insights into the formation of the active site. *Nucleic Acids Res. 39*, 4427−4437.
(37) Jones, F. D., and Strobel, S. A. (2003) Ionization of a critical adenosine residue in the *Neurospora* Varkud satellite ribozyme active site. *Biochemistry 42*, 4265−4276.
(38) McLeod, A. C., and Lilley, D. M. (2004) Efficient, pH-dependent RNA ligation by the VS ribozyme in trans. *Biochemistry 43*, 1118−1125.
(39) Zhao, Z. Y., McLeod, A., Harusawa, S., Araki, L., Yamaguchi, M., Kurihara, T., and Lilley, D. M. (2005) Nucleobase participation in ribozyme catalysis. *J. Am. Chem. Soc. 127*, 5026−5027.
(40) Smith, M. D., and Collins, R. A. (2007) Evidence for proton transfer in the rate-limiting step of a fast-cleaving Varkud satellite ribozyme. *Proc. Natl. Acad. Sci. U.S.A. 104*, 5818−5823.
(41) Jaikaran, D., Smith, M. D., Mehdizadeh, R., Olive, J., and Collins, R. A. (2008) An important role of G638 in the cis-cleavage reaction of the *Neurospora* VS ribozyme revealed by a novel nucleotide analog incorporation method. *RNA 14*, 938−949.
(42) Smith, M. D., Mehdizadeh, R., Olive, J. E., and Collins, R. A. (2008) The ionic environment determines ribozyme cleavage rate by modulation of nucleobase pKa. *RNA 14*, 1942−1949.
(43) Wilson, T. J., Li, N. S., Lu, J., Frederiksen, J. K., Piccirilli, J. A., and Lilley, D. M. (2010) Nucleobase-mediated general acid-base catalysis in the Varkud satellite ribozyme. *Proc. Natl. Acad. Sci. U.S.A. 107*, 11751−11756.
(44) Lafontaine, D. A., Norman, D. G., and Lilley, D. M. (2001) Structure, folding and activity of the VS ribozyme: Importance of the 2-3-6 helical junction. *EMBO J. 20*, 1415−1424.
(45) Lafontaine, D. A., Norman, D. G., and Lilley, D. M. (2002) The global structure of the VS ribozyme. *EMBO J. 21*, 2461−2471.
(46) Sood, V. D., and Collins, R. A. (2001) Functional equivalence of the uridine turn and the hairpin as building blocks of tertiary structure in the *Neurospora* VS ribozyme. *J. Mol. Biol. 313*, 1013−1019.
(47) Tyagi, R., and Mathews, D. H. (2007) Predicting helical coaxial stacking in RNA multibranch loops. *RNA 13*, 939−951.
(48) Lipfert, J., Ouellet, J., Norman, D. G., Doniach, S., and Lilley, D. M. (2008) The complete VS ribozyme in solution studied by small-angle X-ray scattering. *Structure 16*, 1357−1367.
(49) Bonneau, E., and Legault, P. (2014) NMR localization of divalent cations at the active site of the *Neurospora* VS ribozyme provides insights into RNA-metal-ion interactions. *Biochemistry 53*, 579−590.
(50) Rastogi, T., and Collins, R. A. (1998) Smaller, faster ribozymes reveal the catalytic core of *Neurospora* VS RNA. *J. Mol. Biol. 277*, 215−224.
(51) Milligan, J. F., Groebe, D. R., Witherell, G. W., and Uhlenbeck, O. C. (1987) Oligoribonucleotide synthesis using T7 RNA polymerase and synthetic DNA templates. *Nucleic Acids Res. 15*, 8783−8798.
(52) Salvail-Lacoste, A., Di Tomasso, G., Piette, B. L., and Legault, P. (2013) Affinity purification of T7 RNA transcripts with homogeneous ends using ARiBo and CRISPR tags. *RNA 19*, 1003−1014.
(53) Nikonowicz, E. P., Sirr, A., Legault, P., Jucker, F. M., Baer, L. M., and Pardi, A. (1992) Preparation of ^{13}C and ^{15}N labelled RNAs for heteronuclear multidimensional NMR studies. *Nucleic Acids Res. 20*, 4507−4513.
(54) Latham, M. P., Brown, D. J., McCallum, S. A., and Pardi, A. (2005) NMR methods for studying the structure and dynamics of RNA. *ChemBioChem 6*, 1492−1505.
(55) Campbell, D. O., and Legault, P. (2005) NMR structure of the Varkud satellite ribozyme stem-loop V RNA and magnesium-ion binding from chemical-shift mapping. *Biochemistry 44*, 4157−4170.
(56) Delaglio, F., Grzesiek, S., Vuister, G. W., Zhu, G., Pfeifer, J., and Bax, A. (1995) NMRPipe: A multidimensional spectral processing system based on UNIX pipes. *J. Biomol. NMR 6*, 277−293.
(57) Vranken, W. F., Boucher, W., Stevens, T. J., Fogh, R. H., Pajon, A., Llinas, M., Ulrich, E. L., Markley, J. L., Ionides, J., and Laue, E. D. (2005) The CCPN data model for NMR spectroscopy: Development of a software pipeline. *Proteins 59*, 687−696.
(58) Heus, H. A., and Pardi, A. (1991) Structural features that give rise to the unusual stability of RNA hairpins containing GNRA tetraloops. *Science 253*, 191−194.
(59) Jucker, F. M., Heus, H. A., Yip, P. F., Moors, E. H., and Pardi, A. (1996) A network of heterogeneous hydrogen bonds in GNRA tetraloops. *J. Mol. Biol. 264*, 968−980.
(60) Kay, L. E., Keifer, P., and Saarinen, T. (1992) Pure absorption gradient enhanced heteronuclear single quantum correlation spectroscopy with improved sensitivity. *J. Am. Chem. Soc. 114*, 10663−10665.
(61) Vuister, G. W., and Bax, A. (1992) Resolution enhancement and spectral editing of uniformly ^{13}C-enriched proteins by homonuclear broadband ^{13}C decoupling. *J. Magn. Reson. 98*, 428−435.
(62) Santoro, J., and King, G. C. (1992) A constant-time 2D overbodenhausen experiment for inverse correlation of isotopically enriched species. *J. Magn. Reson. 97*, 202−207.
(63) Schwieters, C. D., Kuszewski, J. J., Tjandra, N., and Clore, G. M. (2003) The Xplor-NIH NMR molecular structure determination package. *J. Magn. Reson. 160*, 66−74.
(64) Lavery, R., Moakher, M., Maddocks, J. H., Petkeviciute, D., and Zakrzewska, K. (2009) Conformational analysis of nucleic acids revisited: Curves+. *Nucleic Acids Res. 37*, 5917−5929.
(65) Jucker, F. M., and Pardi, A. (1995) Solution structure of the CUUG hairpin loop: A novel RNA tetraloop motif. *Biochemistry 34*, 14416−14427.
(66) Murray, L. J., Arendall, W. B., III, Richardson, D. C., and Richardson, J. S. (2003) RNA backbone is rotameric. *Proc. Natl. Acad. Sci. U.S.A. 100*, 13904−13909.
(67) Campbell, D. O., Bouchard, P., Desjardins, G., and Legault, P. (2006) NMR structure of Varkud satellite ribozyme stem-loop V in the presence of magnesium ions and localization of metal-binding sites. *Biochemistry 45*, 10591−10605.
(68) Woese, C. R., Winker, S., and Gutell, R. R. (1990) Architecture of ribosomal RNA: Constraints on the sequence of "tetra-loops". *Proc. Natl. Acad. Sci. U.S.A. 87*, 8467−8471.
(69) Wolters, J. (1992) The nature of preferred hairpin structures in 16S-like rRNA variable regions. *Nucleic Acids Res. 20*, 1843−1850.
(70) Proctor, D. J., Schaak, J. E., Bevilacqua, J. M., Falzone, C. J., and Bevilacqua, P. C. (2002) Isolation and characterization of a family of

stable RNA tetraloops with the motif YNMG that participate in tertiary interactions. *Biochemistry 41*, 12062−12075.
(71) Antao, V. P., Lai, S. Y., and Tinoco, I., Jr. (1991) A thermodynamic study of unusually stable RNA and DNA hairpins. *Nucleic Acids Res. 19*, 5901−5905.
(72) Baumruk, V., Gouyette, C., Huynh-Dinh, T., Sun, J. S., and Ghomi, M. (2001) Comparison between CUUG and UUCG tetraloops: Thermodynamic stability and structural features analyzed by UV absorption and vibrational spectroscopy. *Nucleic Acids Res. 29*, 4089−4096.
(73) Petrov, A. I., Zirbel, C. L., and Leontis, N. B. (2011) WebFR3D: A server for finding, aligning and analyzing recurrent RNA 3D motifs. *Nucleic Acids Res. 39*, W50−W55.
(74) Schuwirth, B. S., Borovinskaya, M. A., Hau, C. W., Zhang, W., Vila-Sanjurjo, A., Holton, J. M., and Cate, J. H. (2005) Structures of the bacterial ribosome at 3.5 Å resolution. *Science 310*, 827−834.
(75) Pley, H. W., Flaherty, K. M., and McKay, D. B. (1994) Model for an RNA tertiary interaction from the structure of an intermolecular complex between a GAAA tetraloop and an RNA helix. *Nature 372*, 111−113.
(76) Costa, M., and Michel, F. (1995) Frequent use of the same tertiary motif by self-folding RNAs. *EMBO J. 14*, 1276−1285.
(77) Suydam, I. T., and Strobel, S. A. (2008) Fluorine substituted adenosines as probes of nucleobase protonation in functional RNAs. *J. Am. Chem. Soc. 130*, 13639−13648.
(78) Sood, V. D., Yekta, S., and Collins, R. A. (2002) The contribution of 2′-hydroxyls to the cleavage activity of the *Neurospora* VS ribozyme. *Nucleic Acids Res. 30*, 1132−1138.
(79) Wimberly, B. T., Brodersen, D. E., Clemons, W. M., Jr., Morgan-Warren, R. J., Carter, A. P., Vonrhein, C., Hartsch, T., and Ramakrishnan, V. (2000) Structure of the 30S ribosomal subunit. *Nature 407*, 327−339.
(80) Klein, D. J., Moore, P. B., and Steitz, T. A. (2004) The roles of ribosomal proteins in the structure assembly, and evolution of the large ribosomal subunit. *J. Mol. Biol. 340*, 141−177.
(81) Conn, G. L., Gittis, A. G., Lattman, E. E., Misra, V. K., and Draper, D. E. (2002) A compact RNA tertiary structure contains a buried backbone-K^+ complex. *J. Mol. Biol. 318*, 963−973.
(82) Weichenrieder, O., Wild, K., Strub, K., and Cusack, S. (2000) Structure and assembly of the Alu domain of the mammalian signal recognition particle. *Nature 408*, 167−173.
(83) Kuglstatter, A., Oubridge, C., and Nagai, K. (2002) Induced structural changes of 7SL RNA during the assembly of human signal recognition particle. *Nat. Struct. Biol. 9*, 740−744.
(84) Scott, W. G., Finch, J. T., and Klug, A. (1995) The crystal structure of an all-RNA hammerhead ribozyme: A proposed mechanim for RNA catalytic cleavage. *Cell 81*, 991−1002.
(85) Golden, B. L., Kim, H., and Chase, E. (2005) Crystal structure of a phage Twort group I ribozyme-product complex. *Nat. Struct. Mol. Biol. 12*, 82−88.
(86) Wu, H., and Feigon, J. (2007) H/ACA small nucleolar RNA pseudouridylation pockets bind substrate RNA to form three-way junctions that position the target U for modification. *Proc. Natl. Acad. Sci. U.S.A. 104*, 6655−6660.
(87) Pikovskaya, O., Polonskaia, A., Patel, D. J., and Serganov, A. (2011) Structural principles of nucleoside selectivity in a 2′-deoxyguanosine riboswitch. *Nat. Chem. Biol. 7*, 748−755.
(88) Huang, L., Ishibe-Murakami, S., Patel, D. J., and Serganov, A. (2011) Long-range pseudoknot interactions dictate the regulatory response in the tetrahydrofolate riboswitch. *Proc. Natl. Acad. Sci. U.S.A. 108*, 14801−14806.
(89) Donghi, D., Pechlaner, M., Finazzo, C., Knobloch, B., and Sigel, R. K. (2013) The structural stabilization of the κ three-way junction by Mg(II) represents the first step in the folding of a group II intron. *Nucleic Acids Res. 41*, 2489−2504.
(90) Chapman, E. G., Costantino, D. A., Rabe, J. L., Moon, S. L., Wilusz, J., Nix, J. C., and Kieft, J. S. (2014) The structural basis of pathogenic subgenomic flavivirus RNA (sfRNA) production. *Science 344*, 307−310.